Spectral predictors*

Peter Lindstrom
Lawrence Livermore National Laboratory
pl@llnl.gov

Jarek Rossignac, Lorenzo Ibarria
Georgia Institute of Technology
{jarek, redark}@cc.gatech.edu

Abstract

Many scientific, imaging, and geospatial applications produce large high-precision scalar fields sampled on a regular grid. Lossless compression of such data is commonly done using predictive coding, in which weighted combinations of previously coded samples known to both encoder and decoder are used to predict subsequent nearby samples. In hierarchical, incremental, or selective transmission, the spatial pattern of the known neighbors is often irregular and varies from one sample to the next, which precludes prediction based on a single stencil and fixed set of weights. To handle such situations and make the best use of available neighboring samples, we propose a local *spectral* predictor that offers optimal prediction by tailoring the weights to each configuration of known nearby samples. These weights may be precomputed and stored in a small lookup table. We show that predictive coding using our spectral predictor improves compression for various sources of high-precision data.

1 Introduction

The acquisition or computation of most scientific datasets [CCW*05], high dynamic range images [Lar98], and videos usually requires a significant amount of effort and computing resources. Yet, their exploitation is often hindered by the mismatch between the size of the files in which they are stored and the available bandwidth for downloading or visualizing them. Although the loss of precision resulting from a controlled quantization or lossy compression may be acceptable for visualization purposes, lossless compression of integer or floating-point values is required in many settings to guarantee the integrity of the data, especially if it is to be used to save state in "restart dumps" to allow resuming an interrupted simulation [CCW*05]. Furthermore, it is often desired that the data be compressed as it is created, streamed, and decompressed using a small memory footprint.

*This work was performed under the auspices of the U.S. DOE by LLNL under contract W-7405-Eng-48.

Although traditional image compression techniques are capable of lossless compression [WSS00, Roe03], they were developed for the media industry which usually deals with low-precision data and tolerates trading some accuracy for increased compression. In contrast, we focus on the lossless compression of high-precision data sets represented for example as 32-bit integers or floating-point numbers.

Several predictive coding approaches for structured datasets have been proposed [KB74, Fer87,ILRS03]. We improve on these approaches by proposing a new predictor particularly well suited for the compression of highly precise samplings of smooth scalar fields.

The compression and streaming approach investigated here follow a simple paradigm: compute the prediction $p_{i,j}$ of the scalar value $f_{i,j}$ from values of previously processed samples in the neighborhood $N_{i,j}$; compress the corrections, $c_{i,j} = f_{i,j} - p_{i,j}$, using lossless entropy coding or a custom format designed for compactly encoding differences between nearby floating-point numbers; and stream them. The paradigm leads to simplicity of implementation, small memory footprint, and excellent compression.

Although our framework is general enough to handle larger neighborhoods and unstructured and higher-dimensional data, we limit our attention in this paper to prediction within 3×3 neighborhoods. When the predicted sample is at a corner of a full neighborhood (all eight neighbors known), our spectral predictor reduces to the extrapolating *bi-Lorenzian* predictor; an extension of the previously proposed Lorenzo predictor suited for scanline transmission. When the predicted sample is at the center of a full neighborhood, we obtain the *radial* interpolating predictor, which is four times more accurate than the bi-Lorenzian and is useful in hierarchical transmission. We show that the spectral predictor leads to smaller residuals than other predictors that use a 3×3 neighborhood for lossless compression of high-precision floating-point or integer data. We also explain how to select a priori the best of the nine possible 3×3 neighborhoods that contain the sample to be predicted.

2 Extrapolating Bi-Lorenzian Predictor, L^2

Before we derive our spectral predictor, we begin by considering the L^1 Lorenzo predictor [ILRS03]. Let f be a one-dimensional function regularly sampled at $\{\ldots, f_{i-1}, f_i, f_{i+1}, \ldots\}$, and let Δ^x be the finite difference $\Delta^x_i = f_i - f_{i-1}$. That is, Δ^x is an approximation of the differential $\frac{\partial f}{\partial x}\,dx$. Setting $\Delta^x_i = 0$, solving for f_i, and substituting L^1_i for f_i, we have as 1D Lorenzo predictor $L^1_i = f_{i-1}$. The Lorenzo predictor extends to 2D via composition of derivatives: $\Delta^{xy}_{i,j} = \Delta^x_{i,j} - \Delta^x_{i,j-1} = f_{i-1,j-1} - f_{i,j-1} - f_{i-1,j} + f_{i,j}$. As the sampling rate of f increases, Δ^{xy} approaches $\frac{\partial^2 f}{\partial x \partial y}\,dx\,dy$ in the limit. Setting $\Delta^{xy}_{i,j} = 0$, we can now express the 2D Lorenzo predictor as

$$L^1_{i,j} = f_{i,j-1} + f_{i-1,j} - f_{i-1,j-1} \tag{1}$$

Thus, in the limit, L^1 correctly predicts all continuous functions f with $\frac{\partial^2 f}{\partial x \partial y} = 0$. In the discrete setting, L^1 recovers linear polynomials, or equivalently bilinear polynomials without highest order term xy. Figure 1(a) shows how the 2D Lorenzo predictor estimates the sample indicated by '?' as a weighted sum of three of its neighbors. We have successfully used L^1 in higher dimensions to predict regular grids [ILRS03].

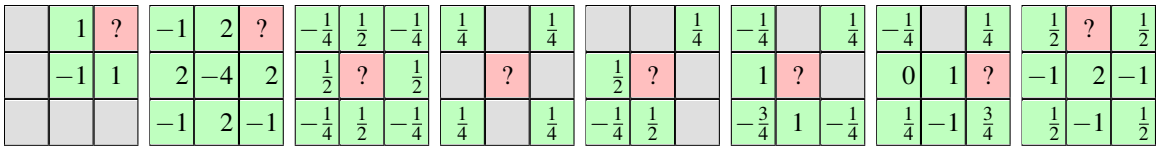

(a) L^1 (b) L^2 (c) R (d) B (e) H (f) S_f (g) S_v (h) S_h

Figure 1: Weights for several spectral predictors used in our experiments: (a) Lorenzo, (b) bi-Lorenzian, (c) radial, (d) bilinear, (e) hybrid linear and radial, (f–h) full spectral.

It is natural to ask whether the Lorenzo predictor can be extended to higher-order polynomials that have vanishing higher-order derivatives. To accomplish this, we take finite differences once more and obtain

$$\begin{aligned}\Delta^{xxyy}_{i,j} &= \Delta^{xy}_{i,j} - \Delta^{xy}_{i+1,j} - \Delta^{xy}_{i,j+1} + \Delta^{xy}_{i+1,j+1} \\ &= 2f_{i,j-1} + 2f_{i-1,j} + 2f_{i+1,j} + 2f_{i,j+1} - 4f_{i,j} \\ &\quad - f_{i-1,j-1} - f_{i+1,j-1} - f_{i-1,j+1} - f_{i+1,j+1}\end{aligned}$$

where we define Δ^{xxyy} using central differences. Setting $\Delta^{xxyy}_{i,j} = 0$ and solving for $f_{i+1,j+1}$ we obtain the *bi-Lorenzian* predictor

$$L^2_{i+1,j+1} = 2f_{i,j-1} + 2f_{i-1,j} + 2f_{i+1,j} + 2f_{i,j+1} - 4f_{i,j} - f_{i-1,j-1} - f_{i+1,j-1} - f_{i-1,j+1} \quad (2)$$

In the limit, L^2 reproduces functions f with $\frac{\partial^4 f}{\partial x^2 \partial y^2} = 0$, and in the discrete setting interpolates biquadratic polynomials without highest order term x^2y^2. Whereas Δ^{xxyy} relates to Δ^{xy} as Δ^{xy} relates to f, L^2 is usually not the successive application of L^1, i.e. in general $L^2_{i,j} \neq L^1_{i,j-1} + L^1_{i-1,j} - L^1_{i-1,j-1}$. Instead, L^2 may be derived by setting to zero the L^1 correction of the L^1 corrections at (i, j). The L^2 weights are shown in Figure 1(b).

The L^1 predictor has been widely used in the image and geometry compression communities [TG98, ILRS03, WSS00, Roe03]. We are, however, not aware of its extension L^2 having been used for compression of 2D and higher-dimensional data.

3 Interpolating Predictor, R

In the previous section we presented an extrapolating predictor, L^2, for a corner $f_{i+1,j+1}$ of a 3×3 neighborhood of samples. This predictor arose from the constraint $\Delta^{xxyy}_{i,j} = 0$, a central difference evaluated at the *center* sample of this neighborhood. A more effective predictor is obtained by solving Equation 2 for the function value at the center sample $f_{i,j}$, which results in the *radial* interpolating predictor

$$\begin{aligned}R_{i,j} = \frac{1}{4}\big(&2f_{i,j-1} + 2f_{i-1,j} + 2f_{i+1,j} + 2f_{i,j+1} \\ &- f_{i-1,j-1} - f_{i+1,j-1} - f_{i-1,j+1} - f_{i+1,j+1}\big)\end{aligned} \quad (3)$$

We use the term "radial" to describe this predictor because its weights are radially dependent on the distance to neighboring samples (Figure 1(c)). The predicted value $R_{i,j}$ is

$2E - C$ where E is the mean of the four edge neighbors and C is the mean of the four corner neighbors. $R_{i,j}$ also equals the mean of the four possible L^1 predictions of $f_{i,j}$.

R has the same predictive power as L^2, i.e. it reproduces biquadratics with no x^2y^2 term, but typically yields better predictions due to the symmetric configuration of its neighborhood. Using Taylor expansion of f one can show that the prediction error of L^2 is $\frac{\partial^4 f}{\partial x^2 \partial y^2}$ (plus higher order terms), which is four times larger than the prediction error for R. Note that to use R, we either must know all eight surrounding neighbors or must estimate them via alternative predictors.

4 Spectral Predictor, S

Our spectral predictor S generalizes L^2 and R to all possible configurations of 0 to 8 known samples and locations of the predicted sample in a 3×3 neighborhood. As in image compression methods based on discrete wavelet [CO97] and cosine transforms [Wal91], we captialize on the fact that the signal power is often heavily skewed towards low frequencies. In frequency transforms, this results in small, compressible high-frequency detail coefficients, whereas in predictive coding "smooth" interpolants recover most of the low-frequency response, leading to small correctors for the missing high-frequency content.

In this section, we design as-smooth-as-possible interpolants for irregular sample configurations. We seek to eliminate or, when not possible, to minimize high-frequency responses in the interpolant. The resulting predictors and their sets of weights are straightforward to use in a compression scheme, and can be stored in a lookup table indexed by the mask of known and unknown values and the location of the predicted sample.

We build upon the work by Isenburg et al. [IIGS05], who use the Fourier transform to predict the geometry of n-sided polygons to be "as regular as possible" given $m < n$ known vertices. They express the vertex coordinates of the polygon in the complex plane, apply the discrete Fourier transform (DFT) to this n-vector of consecutive vertex coordinates, set the highest $n - m$ frequencies to zero, and compute the inverse transform to obtain the complex coordinates of the predicted vertices. Because the Fourier transform is linear, the unknown vertices can be expressed in terms of a linear combination of the known vertices. By working out the mathematics of the forward and inverse Fourier transforms, one can a priori establish a set of weights to be used for a given configuration (m,n) of known and unknown number of vertices (i.e. the weights are not dependent on the geometry of the known samples). Because Fourier frequencies come in pairs, this approach works well when m is odd as then the resulting weights are guaranteed to be real. One can show that the discrete cosine transform (DCT) can instead be used when m is even. Lifting the DFT to higher dimensions, Isenburg et al. further showed that the L^1 predictor from Section 2 is in the spectral sense the optimal predictor (i.e. smoothest interpolant) for hypercube-like neighborhoods with one unknown sample.

We begin by extending the general approach of Isenburg et al. to 3×3 neighborhoods to re-derive the bi-Lorenzian and radial predictors and show that they are optimal. We will make use of the two-dimensional (orthonormal) discrete cosine basis, shown unnormalized in Figure 2. We unfold the 3×3 matrix into a single 9-dimensional vector $b = \begin{bmatrix} f_{i-1,j-1} & f_{i,j-1} & f_{i+1,j-1} & \cdots & f_{i+1,j+1} \end{bmatrix}^T$ of sample values, and write the cosine

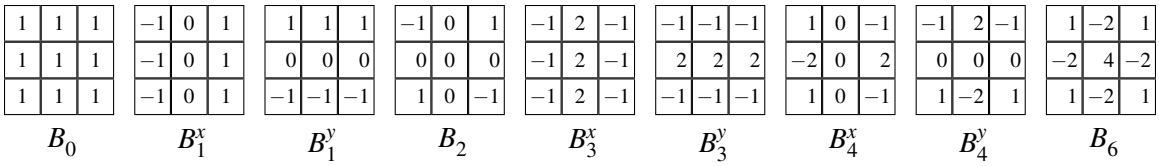

Figure 2: Basis functions for the 2D discrete cosine transform (not normalized).

basis as a 9×9 orthogonal matrix B, where the columns of B are the basis functions. Then the forward discrete cosine transform is simply $x = B^T b$, with x being the DCT coefficients in order of increasing frequency.

To extend the ideas of Isenburg et al. from 1D to 2D, we must rank the basis functions by increasing frequency. The cosine basis formulation gives us pairs of frequencies (ν_x, ν_y) for the horizontal and vertical direction, which must be consolidated into single frequencies. We approach this by deriving the cosine basis through eigenanalysis of the symmetric combinatorial graph Laplacian $\mathcal{L}$ (also called the Kirchoff matrix [Zha04])

$$l_{ij} = \begin{cases} \deg(i) & \text{if } i = j \\ -1 & \text{if } i \text{ and } j \text{ are adjacent} \\ 0 & \text{otherwise} \end{cases} \tag{4}$$

where we consider the graph formed by the 3×3 neighborhood in isolation, with vertical and horizontal edges between adjacent samples. Here $\deg(i)$ denotes the degree or number of neighbors of a sample i, e.g. $\deg(i)$ is 2 for corner samples, 3 for edge samples, and 4 for face samples. As noted by Taubin [Tau95], the eigenbasis of the normalized (asymmetric) Laplacian coincides with the Fourier basis, and the eigenvalues $\{\lambda_i\}$ of $\mathcal{L}$ correspond to frequencies. The above un-normalized (symmetric, positive semidefinite) Laplacian $\mathcal{L}$ has real non-negative eigenvalues $\{0,1,1,2,3,3,4,4,6\}$ and the cosine basis as eigenbasis. We will use B_λ to denote the eigenvector (i.e. basis function) with corresponding eigenvalue λ, and B_λ^x and B_λ^y to distinguish pairs of eigenvectors with equal eigenvalues (Figure 2).

Our formulation shows that there is a unique highest frequency $\lambda = 6$ with associated basis function B_6. Given the eight known samples in the bi-Lorenzian and radial predictors, similarly to Isenburg et al., we set the highest frequency response x_6 to zero and solve for the unknown sample as a linear combination of the $m = 8$ known samples, which results in the weights given in Equations 2 and 3 for corner and center predictions. When $m < 8$, a similar strategy is possible by zeroing $9 - m$ of the highest frequencies. However, we may need to resolve two issues: (1) The $9 - m$ first basis functions may not form a basis for the set of known samples, e.g. $\{B_0, B_1^x, B_1^y\}$ is not a basis for $b = \begin{bmatrix} f_{i-1,j-1} & f_{i,j-1} & f_{i+1,j-1} & 0 & \cdots & 0 \end{bmatrix}^T$. (2) In situations when only one of B_λ^x and B_λ^y is needed (e.g. when exactly two samples are known), we may reduce the total frequency response by choosing a linear combination of B_λ^x and B_λ^y.

Let M be an $m \times n$ mask matrix that extracts the m known samples Mb from b, i.e. each row of M has a single one entry and remaining zeros. We wish to solve the underconstrained system $MBx = Mb$ for x with as many high frequencies of x zeroed as possible. This can be done via linearly constrained least-squares methods, which involves symbolic inversion of an $(m+n) \times (m+n)$ matrix. We show here how to accomplish the same goal via inversion of a smaller $m \times m$ matrix.

$$M = \begin{bmatrix} 1 & 0 & 0 & 0 & 0 & 0 & 0 & 0 & 0 \\ 0 & 0 & 0 & 0 & 0 & 1 & 0 & 0 & 0 \end{bmatrix} \quad P^T = \begin{bmatrix} 1 & 0 & 0 & 0 & 0 & 0 & 0 & 0 & 0 \\ 0 & \frac{2}{\sqrt{5}} & \frac{1}{\sqrt{5}} & 0 & 0 & 0 & 0 & 0 & 0 \end{bmatrix}$$

Figure 3: Example mask matrix M, interpolation matrix P, and predictor weights.

We first must find an m-dimensional basis for Mb by selecting from or combining the $n > m$ column vectors MB; any excluded vector from MB will implicitly have its corresponding frequency response zeroed. Our approach is to incrementally construct an $n \times m$ interpolation matrix P that linearly combines vectors from MB such that $MBPy = Mb$ is a fully constrained system of m equations, with $x = Py$. We achieve this by adding to P columns that select basis functions from MB in order of increasing frequency λ. If a basis function projected onto the space of known samples is redundant (linearly dependent) with respect to the partially constructed basis, we exclude it and consider the next basis function. When we encounter an eigenspace, i.e. two basis functions with the same eigenvalue, one of three situations arises: (1) The whole eigenspace is redundant, and we exlude it. (2) The whole eigenspace is nonredundant, and we include it. (3) The eigenspace is partially redundant, in which case we first "rotate" the eigenspace by an angle θ to make one of the rotated and projected basis functions redundant. (Note that any rotation of an eigenspace preserves eigenvalues and orthogonality with the rest of the basis.) This leaves a nonredundant basis function $B_\lambda^\theta = \cos(\theta)B_\lambda^x + \sin(\theta)B_\lambda^y$ and we add to P a column that has $\cos(\theta)$ and $\sin(\theta)$ in the rows corresponding to B_λ^x and B_λ^y. The effect of this rotation is to "align" the basis function with the spatial configuration of known samples. One can show that this rotation leads to the minimal total frequency response $||x||$.

We may now compute $x = P(MBP)^{-1}Mb$ using matrix inversion. We are, however, not interested in the frequency response x but in the weights of the known samples Mb. Hence we apply the inverse DCT to x and compute $Bx = Wb$, where W is the $n \times n$ weight matrix $W = BP(MBP)^{-1}M$, which is then used to predict unknown samples in b from known ones.

We have implemented this method symbolically in Mathematica and computed exact weights W for all neighborhood configurations, resulting in 41 unique weights in the range $[-4, +4]$ that are predominantly integers and otherwise rationals. This list of weights can be found at `http://www.cc.gatech.edu/~lindstro/data/spectral/`. Note that our weights always add to unity, making our predictor affine invariant.

4.1 Choosing a Neighborhood

Via translation we can form nine 3×3 neighborhoods around each predicted sample p. Depending on the configuration of known samples it is not immediately clear which neighborhood to predict from. We propose training the compressor on the given data set: each of the 9×2^8 predictors is exercised on each sample and receives a ranking based on the mean error it makes. This short ranking is transmitted before compression begins and determines the choice of predictor. In Figure 7 we show using random sampling of several data sets that our approach improves upon: using the neighborhood centered at p, and using the mean or the median of all nine predictions. For calibration, we also report the results for the best (lowest residual) of the nine neighborhoods (which unfortunately is not available to the decoder), as well as the mean and median of constant (single-value) and L^1 prediction.

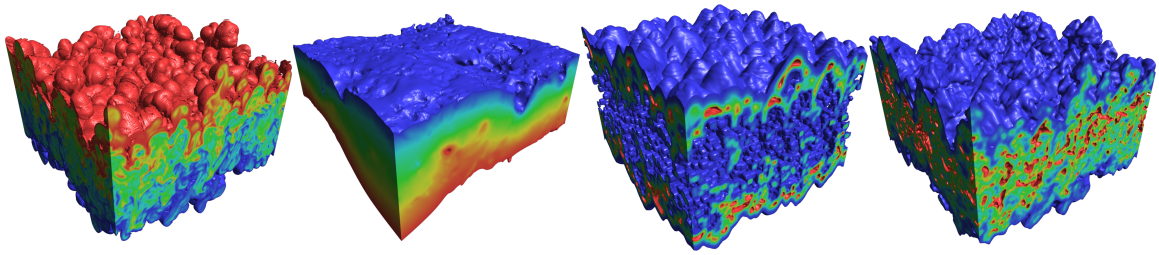

(a) density *(b) pressure* *(c) diffusivity* *(d) viscocity*

Figure 4: Interval-volume renderings of the 3D scalar fields used in our experiments.

5 Applications of Spectral Prediction

Our spectral predictor is particularly useful in applications where standard compression techniques, e.g. based on wavelets, are not practical, such as for encoding data sets with irregular domains due to manual or automatic extraction, inpainting, selective updates, adaptive sampling, or range queries that extract those samples whose values fall within an interval. Irregular sample configurations also arise when the data is traversed in other than scanline order, or in mesh compression, where the domain connectivity is inherently irregular. For lack of space, we here consider only a few of these applications.

We evaluate predictor performance in terms of the number of significant corrector bits, which is the dominating cost in predictive coders for high-precision data [EFF00, RKB06], including our own [LI06]. For floating-point data, the integer corrector measures the number of distinct floating-point values between the actual and predicted value.

5.1 Scanline Transmission

The most straightforward method to compress regularly gridded data is to make a scanline traversal, e.g. row-by-row from bottom to top and from left to right within each row. We here compare our bi-Lorenzian L^2 predictor with other scanline predictors proposed for image compression: the Paeth predictor used in the PNG image format [Roe03], the median predictor used in JPEG-LS [WSS00], and the L^1 Lorenzo predictor [ILRS03]. All except L^2 predict a sample from the same set of three neighbors (Figure 1(a)).

In order to apply L^2 in a scanline traversal, two rows of previously coded samples must be maintained (Figure 6(a)). To bootstrap the predictor, one may use lower-dimensional Lorenzo prediction to first recover domain boundaries. Alternatively, one may use the spectral predictor for partially known neighborhoods described in Section 4.

Figure 5(a) shows the results of predicting multiple 2D slices of single-precision floating-point scalar fields from a fluid dynamics simulation [CCW*05]. On high-precision data like this, L^2 often offers substantially better prediction than predictors that use smaller stencils. The benefit of a larger stencil comes at the expense of higher sensitivity to quantization, however, due to accumulation of per-sample errors and larger (in magnitude) weights. Analysis shows that the prediction error due to quantization is three times larger for L^2 than for L^1. Hence L^2 generally performs worse than L^1 on low-precision data such as 8-bit images.

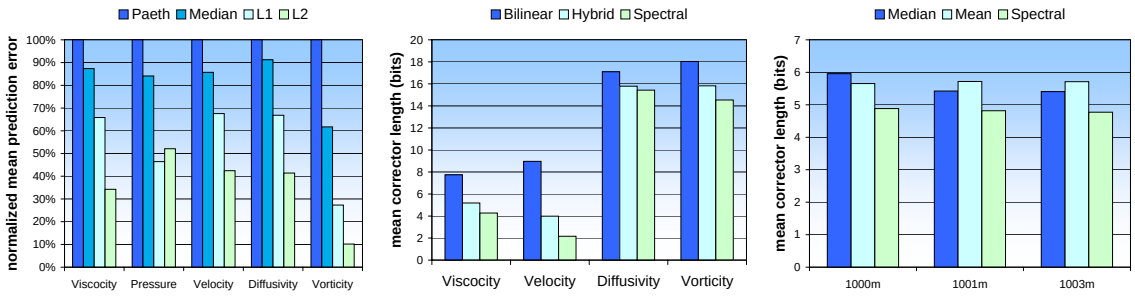

(a) Scanline transmission *(b) Progressive refinement* *(c) Isocontouring*

Figure 5: Prediction results for three different applications.

5.2 Progressive Refinement

Often, data sets are transmitted progressively, doubling the resolution in x and y after each refinement. The missing values within a refinement level may be transmitted in scanline order, as shown in Figure 6(b), which results in three 3×3 neighborhood configurations from which samples are predicted (Figure 6(b–d)).

We consider three predictors for the face sample (Figure 6(c)): bilinear interpolation B of corner samples (Figure 1(d)), spectral prediction S_f (Figure 1(f)), and a hybrid predictor H (Figure 1(e)) that first linearly interpolates the unknown neighbors at the vertical and horizontal edges from their immediate neighbors to fill the neighborhood and then predicts the face point using radial prediction R. Note that both B and H are instances of spectral prediction that simply ignore some of the known neighbors. For the edge points, B and H resort to linear interpolation of corner points for prediction (since no other reasonable non-spectral predictor is available), while our spectral predictor is able to make use of all decoded samples (Figures 1(g) and 1(h)).

Figure 5(b) illustrates the advantage of using all known neighboring samples in the prediction. S_f offers in all cases superior prediction over B and H, leading in one case to as much as a 4:1 improvement in compression. Note that one may choose a different traversal order within each level. In fact, our experiments show that transmitting the missing edge samples first and then the face samples further improves compression, in part because the face samples may be predicted using the radial predictor with fully known (not simply estimated) neighborhoods.

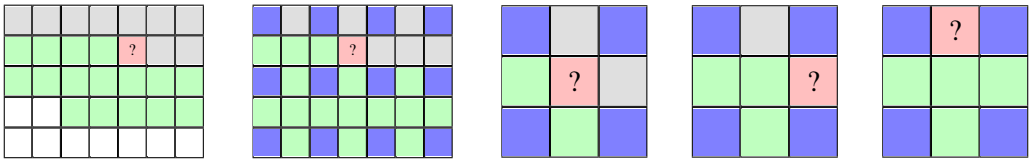

(a) *(b)* *(c)* *(d)* *(e)*

Figure 6: (a) L^2 footprint (green) maintained during scanline traversal. (b) Coarse-resolution (blue) and fine-resolution (green) processed samples in a hierarchical traversal. Within each level of resolution, scanline traversal is used, resulting in three predictor stencils: (c) face, (d) vertical edge, and (e) horizontal edge sample.

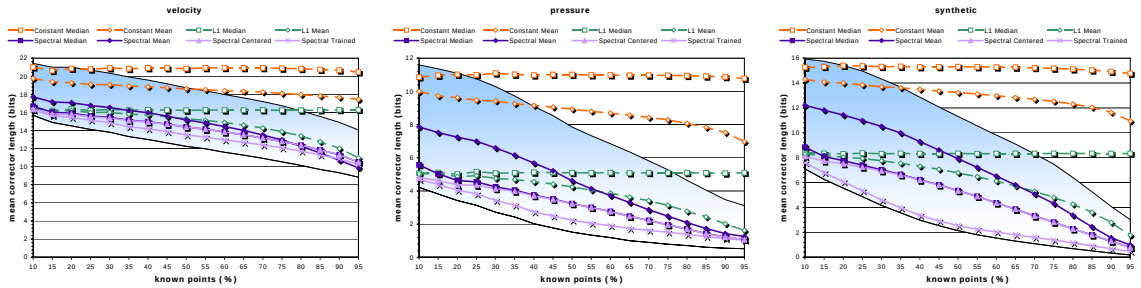

Figure 7: Predictor quality as a function of number of known points in the 3×3 neighborhood. The shaded area indicates the range between best and worst spectral prediction.

5.3 Isocontouring

In many scientific, engineering, and medical applications, regularly sampled volumetric scalar fields are visualized in terms of isosurfaces. For instance, a remote viewer may wish to see the isosurface $S(t)$ formed by all points at temperature t or to explore the family $S(T)$ of isosurfaces with temperatures in a range $T = [t_{min}, t_{max}]$. Instead of transmitting the geometry of $S(t)$ or some compressed form of its animation, it is often more effective to transmit the minimal subset of scalar values needed to reconstruct the single isosurface $S(t)$ or family of isosurfaces $S(T)$ [MIPS03]. To satisfy this query, one needs to transmit not only the samples with values in T, but also some of their neighbors. Furthermore, consider a scenario where the remote user decides to extend T to a larger interval $T \cup R$.

Because we are only interested here in illustrating the benefits of the spectral predictor, we will not discuss the transmission order nor how to encode the mask that identifies the missing samples. We focus on the prediction of the missing values and report experiments of extracting isolines in 2D from the Puget Sound 16-bit terrain surface (available at `http://www.cc.gatech.edu/projects/large_models/ps.html`). We first extracted an isocontour at 1000m elevation and predicted all necessary samples, then incrementally transmitted missing values for isocontours at 1001m and 1003m, resulting in an average number of known neighbors of 5.13, 5.42, and 5.41, respectively. Since samples are often not available for predictors like L^1 to be applied, we compare our spectral predictor with predictions based on the mean and median sample value in a 3×3 neighborhood centered on the predicted sample. We observed consistent reduction in corrector length (13–22%) using the spectral predictor, even for this lower-precision data set (Figure 5(c)).

6 Conclusions

We propose two new predictors, the bi-Lorenzian L^2 and the radial R, which predict the value of a sample f from eight values in a 3×3 neighborhood of which f is the corner (for L^2) or the center (for R). More importantly, we propose the spectral predictor S, which extends L^2 and R to all configurations of known samples and locations of f in a 3×3 neighborhood. We argue that S is the best predictor from a 3×3 neighborhood, provide a strategy for selecting the most promising neighborhood that contains f, and demonstrate the benefits of S over competing predictors in three simple applications.

References

[CCW*05] COOK A. W., CABOT W. H., WILLIAMS P. L., MILLER B. J., DE SUPINSKI B. R., YATES R. K., WELCOME M. L.: Tera-scalable algorithms for variable-density elliptic hydrodynamics with spectral accuracy. In *ACM/IEEE Supercomputing* (2005), p. 60.

[CO97] CHRYSAFIS C., ORTEGA A.: Efficient context-based entropy coding for lossy wavelet image compression. In *Data Compression Conference* (1997), pp. 241–250.

[EFF00] ENGELSON V., FRITZSON D., FRITZSON P.: Lossless compression of high-volume numerical data from simulations. In *Data Compression Conference* (2000), pp. 574–586.

[Fer87] FERIA B. H.: Linear predictive transform of monochrome images. In *IVC* (November 1987), pp. 267–278.

[IIGS05] ISENBURG M., IVRISSIMTZIS I., GUMHOLD S., SEIDEL H.-P.: Geometry prediction for high degree polygons. In *SCCG* (May 2005), pp. 147–152.

[ILRS03] IBARRIA L., LINDSTROM P., ROSSIGNAC J., SZYMCZAK A.: Out-of-core compression and decompression of large *n*-dimensional scalar fields. *Computer Graphics Forum 22*, 3 (Sept. 2003), 343–348.

[KB74] KOBAYASHI H., BAHL L. R.: Image data compression by predictive coding I: Prediction algorithms. In *IBMRD* (March 1974), vol. 2, pp. 164–171.

[Lar98] LARSON G. W.: Logluv encoding for full-gamut, high-dynamic range images. *Journal of Graphics Tools 3*, 1 (1998), 15–31.

[LI06] LINDSTROM P., ISENBURG M.: Fast and efficient compression of floating-point data. *IEEE Transactions on Visualization and Computer Graphics 12*, 5 (Sept. - Oct. 2006), 1245–1250.

[MIPS03] MASCARENHAS A., ISENBURG M., PASCUCCI V., SNOEYINK J.: Encoding volumetric grids for streaming isosurface extraction. In *3DPVT* (2003), pp. 665–672.

[RKB06] RATANAWORABHAN P., KE J., BURTSCHER M.: Fast lossless compression of scientific floating-point data. In *Data Compression Conference* (2006), pp. 133–142.

[Roe03] ROELOFS G.: *PNG: The Definitive Guide*. O'Reilly, 2003. `http://www.libpng.org/pub/png/book/`.

[Tau95] TAUBIN G.: A signal processing approach to fair surface design. In *SIGGRAPH 95* (Aug. 1995), pp. 351–358.

[TG98] TOUMA C., GOTSMAN C.: Triangle mesh compression. In *Graphics Interface* (1998), pp. 26–34.

[Wal91] WALLACE G. K.: The JPEG still picture compression standard. *Communications of the ACM 34*, 4 (1991), 30–44.

[WSS00] WEINBERGER M. J., SEROUSSI G., SAPIRO G.: The LOCO-I lossless image compression algorithm: Principles and standardization into JPEG-LS. *IEEE Transactions on Image Processing 9*, 8 (Aug. 2000), 1309–1324.

[Zha04] ZHANG H.: Discrete combinatorial Laplacian operators for digital geometry processing. In *SIAM Conference on Geometric Design* (2004), pp. 575–592.